

Axion effects on gamma-ray spectral irregularities. II: Implications of EBL absorption

Hai-Jun Li,^{1,*} Wei Chao,^{2,3,†} Xiu-Hui Tan,^{1,‡} and Yu-Feng Zhou^{1,4,5,6,§}

¹Key Laboratory of Theoretical Physics, Institute of Theoretical Physics,
Chinese Academy of Sciences, Beijing 100190, China

²Center for Advanced Quantum Studies, School of Physics and Astronomy,
Beijing Normal University, Beijing 100875, China

³Key Laboratory of Multi-scale Spin Physics, Ministry of Education,
Beijing Normal University, Beijing 100875, China

⁴School of Physical Sciences, University of Chinese Academy of Sciences, Beijing 100049, China

⁵School of Fundamental Physics and Mathematical Sciences,

Hangzhou Institute for Advanced Study, UCAS, Hangzhou 310024, China

⁶International Centre for Theoretical Physics Asia-Pacific, Beijing/Hangzhou, China

(Dated: February 19, 2025)

The extragalactic background light (EBL) plays a crucial role in the propagation of high-energy particles throughout the Universe. In this work, we explore the impact of the EBL absorption effect on photon to axionlike particle (ALP) conversions from the very-high-energy gamma-ray spectral irregularities. For our purpose, we select four BL Lac blazars: Markarian 501, 1ES 0229+200, PKS 0301-243, and PKS 0447-439 for analysis. Their redshifts range from approximately 0.03 to 0.34. We first discuss the EBL absorption effect on the gamma-ray spectral energy distributions (SEDs) using three common EBL spectral models: Finke-10, Franceschini-17, and Saldana-Lopez-21. Then we consider the photon-ALP conversions in astrophysical magnetic fields. The best-fit chi-square distributions of these EBL models under the ALP assumption in the ALP parameter $\{m_a, g_{a\gamma}\}$ plane are provided, showing similar distributions. For comparison, we define a new delta chi-square, χ_d^2 , to quantify the difference in chi-square values. The distributions of χ_d^2 and the gamma-ray SEDs corresponding to the maximum delta chi-square, $\chi_{d,\max}^2$, are also presented for comparison. Our results indicate that the influence of these different EBL models is non-dominant at the low-redshift gamma-ray axionscope. In these cases, choosing the latest model, Saldana-Lopez-21, is sufficient. However, as the redshift of the sources increases, this influence becomes more significant.

I. INTRODUCTION

Axions are excellent candidates for new physics. The QCD axion was originally introduced by the Peccei-Quinn (PQ) mechanism to dynamically solve the strong CP problem in the Standard Model (SM) [1–4], meanwhile, it also provides a natural source for cold dark matter (DM) through the misalignment mechanism [5–7]. On the other hand, the axionlike particle (ALP), predicted by a variety of theories [8, 9], is also the attractive DM candidate [10–12], but does not have to solve the strong CP problem. The axion can couple to the photon with the effective Lagrangian

$$\begin{aligned}\mathcal{L} &= \frac{1}{2}\partial_\mu a \partial^\mu a - \frac{1}{2}m_a^2 a^2 - \frac{1}{4}g_{a\gamma} a F_{\mu\nu} \tilde{F}^{\mu\nu} \\ &= \frac{1}{2}\partial_\mu a \partial^\mu a - \frac{1}{2}m_a^2 a^2 + g_{a\gamma} a \mathbf{E} \cdot \mathbf{B},\end{aligned}\tag{1}$$

where a and m_a donate the axion field and axion mass, respectively, $g_{a\gamma}$ is the axion-photon coupling constant, $F_{\mu\nu}$ ($\tilde{F}^{\mu\nu}$) is the (dual) electromagnetic field tensor, \mathbf{E} and \mathbf{B} are the local electric and magnetic field vectors, respectively. In the QCD axion scenario, the axion mass m_a and coupling $g_{a\gamma}$ are interrelated, whereas in the ALP scenario, they are considered independent parameters. Therefore, the ALP has a much wider $\{m_a, g_{a\gamma}\}$ parameter space than the QCD axion. See ref. [13] for the latest ALP-photon limits.

The coupling between the ALPs and very-high-energy (VHE; $\sim \mathcal{O}(100)$ GeV) photons in astrophysical magnetic fields could lead to some detectable signals, such as a reduced TeV opacity of the Universe [14–17]. The VHE gamma-rays from the extragalactic sources, such as blazars, are mainly affected by the extragalactic background light (EBL) absorption effect due to the electron-positron pair production process

$$\gamma_{\text{TeV}} + \gamma_{\text{EBL}} \rightarrow e^- + e^+, \tag{2}$$

* lihaijun@itp.ac.cn

† chaowei@bnu.edu.cn

‡ tanxh@itp.ac.cn

§ yfzhou@itp.ac.cn

where γ_{TeV} and γ_{EBL} are the VHE photons and background photons, respectively. By taking into account the photon-ALP conversions and back-conversions in the simulated astrophysical magnetic fields, the EBL absorption effect can be mitigated, resulting in the Universe that is potentially more transparent than previously thought solely based on the EBL absorption [18, 19]. Furthermore, it also offers a natural mechanism for constraining ALP properties, and many similar studies have recently been conducted within this axionscope scenario [20–52].

Previous studies show that the source magnetic field parameters, such as the strength of the core magnetic field, have the most significant influence on the limits of ALP properties [30, 32]. Moreover, the source redshift uncertainty has an impact, both the underestimated and overestimated redshifts can affect the ALP limits [53]. Additionally, the EBL absorption effect itself, more precisely, the EBL spectral models, may also have an impact on the final results. However, it can be naively predicted that this effect could be much smaller than those mentioned above, but it is worth investigating them quantitatively.

In this work, we explore the impact of the EBL absorption effect on photon-ALP conversions from the VHE gamma-ray spectral irregularities. In this regard, the gamma-ray source should be selected with a relatively certain redshift. Meanwhile, we should choose different sources for analysis, and the redshift of these sources must vary from low to high. For our purpose, we select four BL Lac blazars: Markarian 501 (with the redshift $z_0 = 0.034$), 1ES 0229+200 (with the redshift $z_0 = 0.1396$), PKS 0301-243 (with the redshift $z_0 = 0.2657$), and PKS 0447-439 (with the redshift $z_0 = 0.343$). Their redshifts vary from $\sim 0.03 - 0.34$, it may be a good choice for us to explore the impact of the EBL absorption effect with these sources. Here we use the relatively latest gamma-ray data of these sources for analysis. See also table I for their position information and the sources of the gamma-ray data. On the other hand, the EBL spectral model should be chosen as a relatively up-to-date one, and there should be certain distinctions among the energy spectra of these models. Therefore, we select three EBL models: Finke-10 [58], Franceschini-17 [59], and Saldana-Lopez-21 [60]. The first EBL spectral model exhibits certain differences from the second and third in the far-infrared regions. Both the second and third models represent the latest EBL models, and the observations for the third model originate from space, offering greater reliability compared to those conducted from the Earth. We first discuss the EBL absorption effect on the gamma-ray spectral energy distributions (SEDs) with these three EBL spectral models. Then we consider the photon-ALP conversions in astrophysical magnetic fields. The best-fit chi-square distributions of these EBL models under the ALP assumption in the ALP parameter $\{m_a, g_{a\gamma}\}$ plane are given, showing similar distributions. For comparison, we define a new delta chi-square χ_d^2 to quantify the chi-square difference. The distributions of χ_d^2 and the gamma-ray SEDs corresponding to the maximum delta chi-square $\chi_{d,\text{max}}^2$ in the $\{m_a, g_{a\gamma}\}$ plane are also shown. Finally, we find that there is only a minor influence from the different EBL models at the low-redshift gamma-ray axionscope. However, as the redshift of the sources increases, this impact becomes more pronounced, which can be observed from the gamma-ray SEDs. On the other hand, the uncertainty in the observed spectra can also directly affect the results. Overall, for the investigation of photon-ALP coupling from the low-redshift gamma-ray sources, choosing the EBL spectral model Saldana-Lopez-21 is sufficient.

The rest of this paper is structured as follows. In section II, we introduce the EBL absorption effect on the VHE gamma-ray propagation and show the gamma-ray data of the selected blazars. In section III, we discuss the photon-ALP conversions in astrophysical magnetic fields. The analysis and results under the ALP assumption are given in section IV. Finally, the conclusion is given in section V.

II. THE GAMMA-RAY SEDS UNDER THE NULL HYPOTHESIS

In this section, we first introduce the EBL absorption effect on the VHE gamma-ray propagation, then we show the gamma-ray SEDs of the selected BL Lac blazars Markarian 501, 1ES 0229+200, PKS 0301-243, and PKS 0447-439.

TABLE I. The redshift and position information of the four BL Lac blazars: Markarian 501, 1ES 0229+200, PKS 0301-243, and PKS 0447-439. See <http://tevcat2.uchicago.edu> for more details. The sources of the gamma-ray data used in this work are also listed.

Source	redshift	Gal.Long. (deg)	Gal.Lat. (deg)	gamma-ray data
Markarian 501	0.034	63.60	38.86	Fermi-LAT+HAWC [54]
1ES 0229+200	0.1396	152.97	-36.61	Fermi-LAT+MAGIC [55]
PKS 0301-243	0.2657	214.63	-60.19	Fermi-LAT+H.E.S.S. [56]
PKS 0447-439	0.343	248.81	-39.91	Fermi-LAT+H.E.S.S. [57]

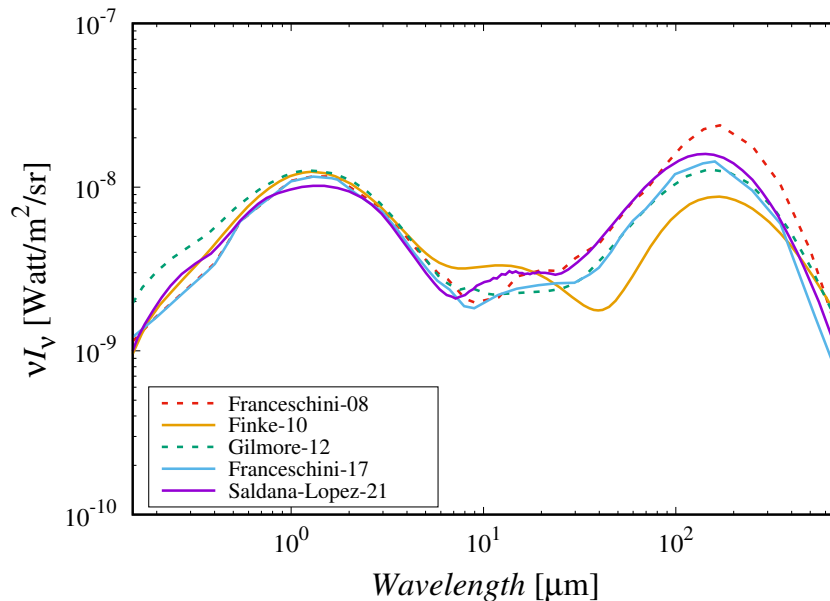


FIG. 1. The EBL spectral models. The lines in different colors represent the spectral models: Franceschini-08 [61], Finke-10 [58], Gilmore-12 [63], Franceschini-17 [59], and Saldana-Lopez-21 [60], respectively. The solid lines represent the three spectral models used in this work.

A. EBL absorption effect

The EBL plays a crucial role in determining the opacity of cosmic high-energy photons and acts as a constraint on the propagation of high-energy particles throughout the Universe. In general, due to eq. (2) the main effect on the VHE photons (with the high-energy E) from the extragalactic space is the EBL photons (with the low-energy ω) absorption effect with the absorption factor $e^{-\tau}$

$$\Phi(E) = e^{-\tau} \Phi_{\text{int}}(E), \quad (3)$$

where $\Phi(E)$ is the gamma-ray expected spectrum, $\Phi_{\text{int}}(E)$ is the intrinsic spectrum, and τ is the optical depth. This optical depth can be described by [61]

$$\tau = c \int_0^{z_0} \frac{dz}{(1+z)H(z)} \int_{E_{\text{th}}}^{\infty} d\omega \frac{dn(z)}{d\omega} \bar{\sigma}(E, \omega, z), \quad (4)$$

with the Hubble expansion rate

$$H(z) = H_0 \sqrt{(1+z)^2 (1 + \Omega_m z) - z(2+z)\Omega_\Lambda}, \quad (5)$$

where z_0 is the source redshift, E_{th} is the threshold energy, $\bar{\sigma}(E, \omega, z)$ is the integral pair-production cross section, $dn(z)/d\omega$ is the EBL proper number density, $H_0 \simeq 67.4 \text{ km s}^{-1} \text{ Mpc}^{-1}$, $\Omega_m \simeq 0.315$, and $\Omega_\Lambda \simeq 0.685$ [62].

In our previous studies, we did not consider different EBL spectral models, but instead opted for a common one. However, in this work, we will take into account the impact of various EBL models. See figure 1 for several common EBL spectral models: Franceschini-08 [61], Finke-10 [58], Gilmore-12 [63], Franceschini-17 [59], and Saldana-Lopez-21 [60]. We can observe that these spectra exhibit similar distributions in the near-infrared regions, but demonstrate distinctly different distributions in the far-infrared regions, especially for the model Finke-10. The energy spectra of the models Gilmore-12 and Franceschini-17 are relatively close overall, with only minor differences in the near-infrared regions. Note that Franceschini-17 is an updated version of Franceschini-08, and compared to the latter, the photon density in the mid-infrared, far-infrared, and sub-millimeter regions of the former's energy spectrum is slightly lower. Unlike the aforementioned models that rely on the Earth's observations, the latest model, Saldana-Lopez-21, adopts a completely new approach based solely on galaxy data to determine the evolving energy spectrum of the EBL, aiming to reduce the current uncertainties associated with high redshifts and infrared intensities. Therefore, this model is more reliable as it can effectively reduce the undesired zodiacal light effect. Additionally, it is noteworthy that there is

another spectral model, CIBER-17 [64], also derived from space observations. However, due to its worse statistical fit and the resulting unrealistic EBL, this model is not considered in our analysis. For our purpose, here the EBL spectral model should be chosen as a relatively up-to-date one, and there should be certain distinctions among the energy spectra of these models. Therefore, we select these three EBL spectral models in this work: Finke-10, Franceschini-17, and Saldana-Lopez-21, corresponding to the yellow, blue, and purple solid lines in figure 1, respectively.

B. The gamma-ray sources and data

As mentioned before, here we should select the gamma-ray source with a relatively certain redshift. Additionally, we should choose various sources for analysis, ensuring that their redshifts range from low to high. We list all currently known BL Lac blazars with certain redshifts in table II, and their redshifts range from 0.031 to 0.695. Among these sources, we select three sources, namely Markarian 501 ($z_0 = 0.034$), 1ES 0229+200 ($z_0 = 0.1396$), and PKS 0301-243 ($z_0 = 0.2657$), with varying redshifts. Furthermore, we find that the two sources with the highest redshifts, 1ES 0033+595 ($z_0 = 0.467$) and PKS 0903-57 ($z_0 = 0.695$), do not have sufficient VHE gamma-ray observation data for ALP analysis, so we chose another source with a higher redshift, PKS 0447-439 ($z_0 = 0.343$). Therefore, in this work we select these four BL Lac blazars: Markarian 501, 1ES 0229+200, PKS 0301-243, and PKS 0447-439 for analysis.

Markarian 501 (R.A. = $16^{\text{h}}53^{\text{m}}52.2^{\text{s}}$, Dec. = $+39^{\circ}45'37''$, J2000) is one of our closest and brightest BL Lac blazars, also known as Mrk 501 and TeV J1653+397. It was first discovered with the VHE emission greater than 300 GeV by the Whipple Observatory Gamma Ray Collaboration in 1996 [65]. Here the used VHE gamma-ray data of Markarian 501 was recently measured by Fermi Large Area Telescope (Fermi-LAT) and High Altitude Water Cherenkov (HAWC) Gamma-Ray Observatory from June 2015 to July 2018 [54].

1ES 0229+200 (R.A. = $02^{\text{h}}32^{\text{m}}53.2^{\text{s}}$, Dec. = $+20^{\circ}16'21''$, J2000) is known for emitting VHE gamma-rays in the hard TeV range, also known as TeV J0232+202. It was first discovered in the Einstein Imaging Proportional Counter (IPC) Slew Survey in 1992 [66] and was later categorized as a BL Lac object in 1993 [67]. In this work, the used VHE gamma-ray observation data of 1ES 0229+200 was recently measured by Fermi-LAT and Major Atmospheric Gamma-ray Imaging Cherenkov (MAGIC) telescopes from September 2013 to December 2017 [55].

PKS 0301-243 (R.A. = $03^{\text{h}}03^{\text{m}}23.49^{\text{s}}$, Dec. = $-24^{\circ}07'35.86''$, J2000), also known as TeV J0303-241. It was first identified as a blazar in 1988 [68] and was later classified as a BL Lac object in 1996 [69]. Here the used VHE gamma-ray data of PKS 0301-243 was measured by Fermi-LAT and High Energy Stereoscopic System (H.E.S.S.) between

TABLE II. BL Lac blazars with certain redshifts, sourced from <http://tevcat2.uchicago.edu>.

Source	redshift	Source	redshift	Source	redshift
Markarian 421	0.031	B2 1811+31	0.117	1ES 0347-121	0.188
Markarian 501	0.034	B3 2247+381	0.1187	RBS 0413	0.19
1ES 2344+514	0.044	TeV J1958-301	0.119329	RBS 0723	0.198
Markarian 180	0.045	RGB J0710+591	0.125	MRC 0910-208	0.19802
1ES 1959+650	0.048	TXS 1515-273	0.1284	1ES 1011+496	0.212
TXS 0210+515	0.049	H 1426+428	0.129	TeV J1224+246	0.218
TeV J1517-243	0.049	1ES 1215+303	0.131	TeV J0238-312	0.232
1ES 2037+521	0.053	TeV J1136+676	0.1342	PKS 0301-243	0.2657
1ES 1727+502	0.055	1ES 0806+524	0.138	1ES 0414+009	0.287
PGC 2402248	0.065	PKS 1440-389	0.1385	OJ 287	0.3056
PKS 0548-322	0.069	1ES 0229+200	0.1396	OT 081	0.322
BL Lacertae	0.069	TeV J1010-313	0.142639	S3 1227+25	0.325
PKS 2005-489	0.071	H 2356-309	0.165	1ES 0502+675	0.34
RGB J0152+017	0.08	TeV J0812+026	0.1721	3C 66A	0.34
1ES 1741+196	0.084	1ES 2322-409	0.1736	PKS 0447-439	0.343
TeV J0013-188	0.095	TeV J2001+438	0.1739	1ES 0033+595	0.467
TeV J1221+282	0.102	TeV J0648+152	0.179	PKS 0903-57	0.695
1ES 1312-423	0.105	1ES 1218+304	0.182		
PKS 2155-304	0.116	1ES 1101-232	0.186		

September 2009 and December 2011 [56].

PKS 0447-439 (R.A. = $04^{\text{h}}49^{\text{m}}28.2^{\text{s}}$, Dec. = $-43^{\circ}50'12''$, J2000) is one of the brightest extragalactic objects listed in the Fermi Bright Source List and exhibits a hard spectrum within the MeV to GeV range, also known as TeV J0449-438. It was first discovered in the radio band in 1981 [70] and was later identified as a bright BL Lac object [71]. Here the used VHE gamma-ray observations data of PKS 0447-439 was measured by Fermi-LAT and H.E.S.S. from November 2009 to January 2010 [57].

See figure 2 for the experimental gamma-ray data of these sources with the blue and red points, respectively.

C. The gamma-ray SEDs

Here we show the gamma-ray SEDs under the null hypothesis. The VHE gamma-ray intrinsic spectrum $\Phi_{\text{int}}(E)$ is selected as the power law with a super-exponential cut-off (SEPWL) model, which can be described by

$$\Phi_{\text{int}}(E) = N_0 (E/E_0)^{-\Gamma} \exp\left(- (E/E_c)^d\right), \quad (6)$$

where N_0 is the normalization constant, Γ is the spectral index, E_c and d are free parameters, and we fix E_0 with a typical value 1 GeV. Then the chi-square value under the null hypothesis is given by

$$\chi_{\text{null}}^2 = \sum_{i=1}^N \left(\frac{e^{-\tau} \Phi_{\text{int}}(E_i) - \psi(E_i)}{\delta(E_i)} \right)^2, \quad (7)$$

where N is the gamma-ray spectral point number, ψ and δ are the detected flux and its uncertainty, respectively. For the experimental data of Markarian 501, 1ES 0229+200, PKS 0301-243, and PKS 0447-439, we have $N = 33, 13, 8,$ and 13 , respectively.

Using the above three EBL spectral models, we show the best-fit gamma-ray SEDs of Markarian 501, 1ES 0229+200, PKS 0301-243, and PKS 0447-439 under the null hypothesis in figure 2. The yellow, blue, and purple lines correspond to the null hypothesis SEDs with the EBL Finke-10, Franceschini-17, and Saldana-Lopez-21, respectively. The best-fit chi-square values obtained with the different EBL spectral models are also listed in table III, and their reduced chi-squares are all less than 2. We find that for the low-redshift source Markarian 501, their distributions are basically the same, except in the high-energy $\sim \mathcal{O}(10)$ TeV region. This is quite understandable, as the attenuation factor is greater at these energies. This effect is more pronounced for the higher-redshift sources, 1ES 0229+200 and PKS 0447-439. However, we find that for PKS 0301-243, the SEDs do not vary significantly among different EBL models. This is mainly because there are relatively few observation points available for this source, and these observation points can be well fitted using different EBL models. In addition, there is a scarcity of high-energy data for this source. Overall, we find that the impact of different EBL spectral models on the SEDs of these sources under the null hypothesis is relatively small, with the exception of the high-energy range.

TABLE III. The best-fit null hypothesis chi-square χ_{null}^2 values of Markarian 501, 1ES 0229+200, PKS 0301-243, and PKS 0447-439 with the EBL spectral models Finke-10, Franceschini-17, and Saldana-Lopez-21.

Source	EBL model	χ_{null}^2	$\chi_{\text{null}}^2/\text{d.o.f.}$
Markarian 501 (33 points)	Finke-10	41.08	1.42
	Franceschini-17	41.09	1.42
	Saldana-Lopez-21	43.07	1.49
1ES 0229+200 (13 points)	Finke-10	2.54	0.28
	Franceschini-17	3.27	0.36
	Saldana-Lopez-21	2.47	0.27
PKS 0301-243 (8 points)	Finke-10	1.77	0.44
	Franceschini-17	1.78	0.45
	Saldana-Lopez-21	1.74	0.44
PKS 0447-439 (13 points)	Finke-10	17.16	1.91
	Franceschini-17	16.18	1.80
	Saldana-Lopez-21	14.36	1.60

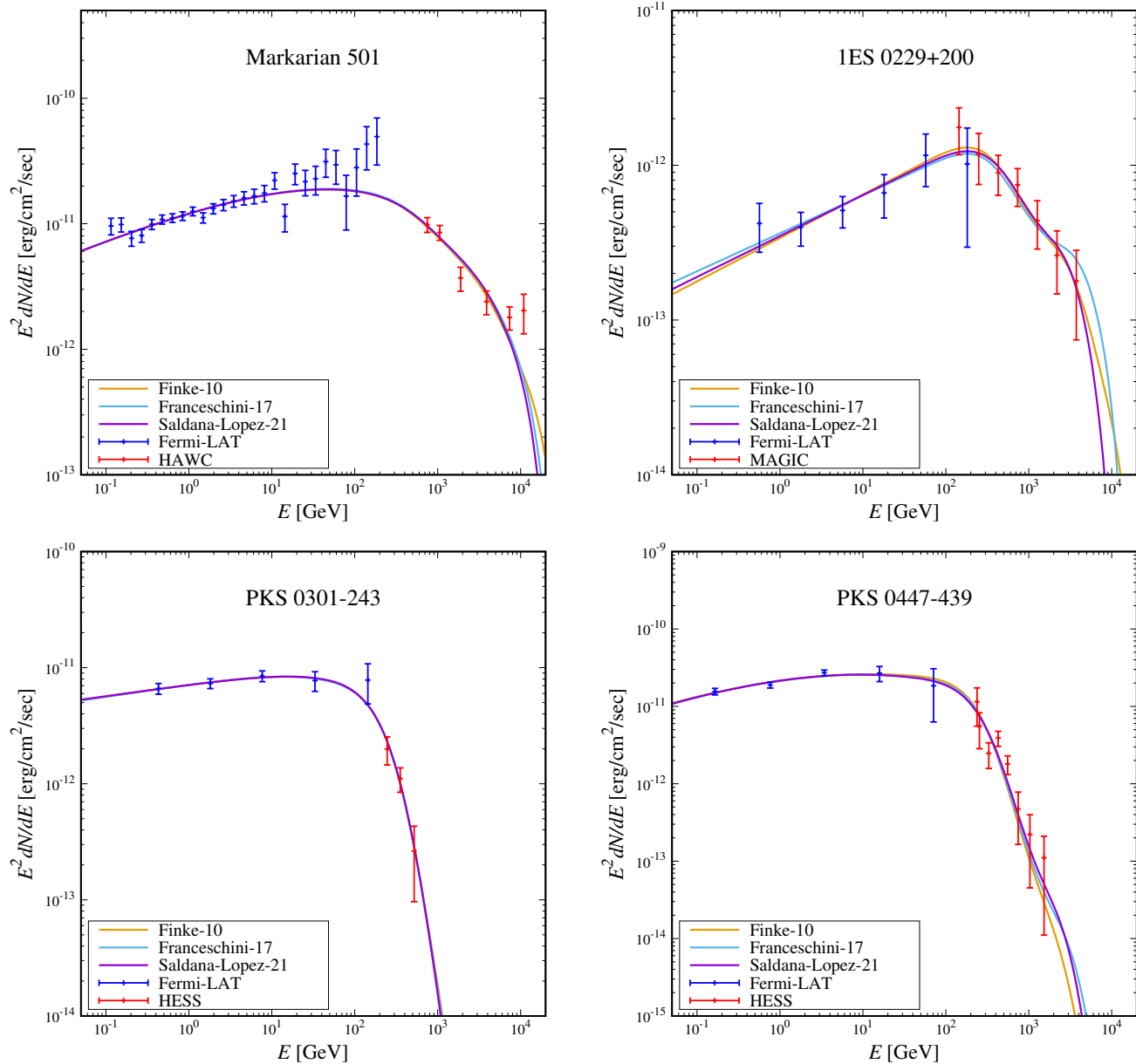


FIG. 2. The best-fit null hypothesis gamma-ray SEDs of Markarian 501, 1ES 0229+200, PKS 0301-243, and PKS 0447-439. The yellow, blue, and purple lines correspond to the SEDs with the EBL spectral models Finke-10, Franceschini-17, and Saldana-Lopez-21, respectively. The blue and red points represent the experimental data.

III. PHOTON-ALP CONVERSIONS IN ASTROPHYSICAL MAGNETIC FIELDS

In this section, we discuss the photon-ALP conversions in astrophysical magnetic fields. We first introduce the photon-ALP conversions in the inhomogeneous magnetic field, then we discuss the setup of astrophysical magnetic field parameters.

A. Photon-ALP conversions in the magnetic field

Before discussing the photon-ALP conversions in the inhomogeneous astrophysical magnetic field, we have already provided the general conversions in the homogeneous magnetic field in appendix A.

In the real astrophysical environment, the magnetic field is inhomogeneous and can be random. In order to obtain

the photon-ALP conversion probability in the inhomogeneous magnetic field, the magnetic field is usually simulated with the domain-like structure and each domain can be regarded as homogeneous. In this case, the photon-ALP system can be described by the density matrix

$$\rho(x_3) = \begin{pmatrix} A_1(x_3) \\ A_2(x_3) \\ a(x_3) \end{pmatrix} \otimes \left(A_1(x_3), A_2(x_3), a(x_3) \right)^* , \quad (8)$$

which satisfies the Von Neumann-like commutator equation

$$i \frac{d\rho(x_3)}{dx_3} = \rho(x_3) \mathcal{M}^\dagger(E, x_3, \theta) - \mathcal{M}(E, x_3, \theta) \rho(x_3), \quad (9)$$

where x_3 is the direction of propagation, A_1 and A_2 are the linear polarization amplitudes of the photon in the perpendicular directions (x_1, x_2), and a is the ALP. Notice that in a case where the transversal magnetic field B_T is not aligned along the direction of x_2 and forms an angle θ , the mixing matrix $\mathcal{M}(E, x_3)$ should be

$$\mathcal{M}(E, x_3) \rightarrow \mathcal{V}^\dagger(\theta) \mathcal{M}(E, x_3) \mathcal{V}(\theta), \quad (10)$$

with

$$\mathcal{V}(\theta) = \begin{pmatrix} \cos \theta & -\sin \theta & 0 \\ \sin \theta & \cos \theta & 0 \\ 0 & 0 & 1 \end{pmatrix}, \quad (11)$$

and we have the mixing matrix

$$\mathcal{M}(E, x_3, \theta) = \begin{pmatrix} \Delta_{11}(E, x_3) & 0 & \Delta_{a\gamma}(x_3) \sin \theta \\ 0 & \Delta_{22}(E, x_3) & \Delta_{a\gamma}(x_3) \cos \theta \\ \Delta_{a\gamma}(x_3) \sin \theta & \Delta_{a\gamma}(x_3) \cos \theta & \Delta_{aa}(E) \end{pmatrix}. \quad (12)$$

The Δ terms in eq. (12) can be found in appendix A within the homogeneous magnetic field. The solution of eq. (9) can be described by

$$\rho(x_3) = \mathcal{T}(E, x_3, \theta) \rho(0) \mathcal{T}^\dagger(E, x_3, \theta), \quad (13)$$

where $\mathcal{T}(E, x_3, \theta)$ is the whole transport matrix of the n domains

$$\mathcal{T}(E, x_3, \theta) = \prod_{i=1}^n \mathcal{T}(E_i, x_{3,i}, \theta_i), \quad (14)$$

and $\rho(0)$ is the initial density matrix

$$\rho(0) = \frac{1}{2} \begin{pmatrix} 1 & 0 & 0 \\ 0 & 1 & 0 \\ 0 & 0 & 0 \end{pmatrix}. \quad (15)$$

Then the photon-ALP-photon conversion probability, or the final photon survival probability, can be described by

$$\mathcal{P}_{\gamma\gamma} = \text{Tr} [(\rho_{11} + \rho_{22}) \mathcal{T}(E, x_3, \theta) \rho(0) \mathcal{T}^\dagger(E, x_3, \theta)], \quad (16)$$

with the matrices

$$\rho_{11} = \begin{pmatrix} 1 & 0 & 0 \\ 0 & 0 & 0 \\ 0 & 0 & 0 \end{pmatrix}, \quad \rho_{22} = \begin{pmatrix} 0 & 0 & 0 \\ 0 & 1 & 0 \\ 0 & 0 & 0 \end{pmatrix}. \quad (17)$$

See also ref. [72] for more details in the calculations. Note that specific analysis is required for the specific magnetic field models. Finally, we can obtain a set of the final photon survival probability $\mathcal{P}_{\gamma\gamma}$.

B. Astrophysical magnetic fields setup

Here we discuss the astrophysical magnetic fields setup associated the photon-ALP beam propagating from the VHE gamma-ray source region to the Earth. Generally, this process is composed of three parts: (1) the source region, (2) the extragalactic space, and (3) the Milky Way.

Firstly, for (1) the source region of the BL Lac object, the blazar jet magnetic field can be described by the poloidal and toroidal components. We consider the photon-ALP conversions in the transverse magnetic field model $B(r) = B_0(r/r_{\text{VHE}})^{-1}$ with the electron density model $n_{\text{el}}(r) = n_0(r/r_{\text{VHE}})^{-2}$, where $r_{\text{VHE}} \sim R_{\text{VHE}}/\theta_{\text{jet}}$ represents the distance between the VHE emission region and the central black hole of the source, R_{VHE} represents the radius of the VHE emission, θ_{jet} represents the angle between the jet axis and the line of sight, B_0 and n_0 represent the core magnetic field and electron density at the distance r_{VHE} , respectively. Since n_0 has a minimal impact on the final result, we take $n_0 = 1 \times 10^3 \text{ cm}^{-3}$ as a typical value in this work. Here we also consider the energy transformation with the Doppler factor, $\delta_{\text{D}} = E_L/E_j$, where E_L and E_j represent the energy in the laboratory and co-moving frames, respectively. For the jet region $r > 1 \text{ kpc}$, the magnetic field is taken as zero. Additionally, for the host galaxy region of the source, the photon-ALP conversion effect can be totally neglected. Then for (2) the extragalactic space, we just need to consider the EBL absorption effect on the VHE gamma-rays due to the electron-positron pair-production process, see also section II A. Since the strength of magnetic field in the extragalactic space is small with the upper limit $\sim \mathcal{O}(1) \text{ nG}$ [73, 74], the photon-ALP conversion effect will be weak, and thus we do not consider the photon-ALP conversions in this part. Finally, in (3) the Milky Way, we should consider the photon-ALP conversions again in the Galactic magnetic field. Generally, this magnetic field can be modeled with the disk and halo components (parallel to the Galactic plane), and the so-called ‘‘X-field’’ component (out-of-plane) at the Galactic center [75, 76]. See also refs. [77, 78] for the latest version of this Galactic magnetic field model.

Here we list the blazar jet magnetic field model parameters B_0 , R_{VHE} , θ_{jet} , r_{VHE} , and δ_{D} of Markarian 501, 1ES 0229+200, PKS 0301-243, and PKS 0447-439 in table IV. On the one hand, some magnetic field parameters are not directly provided; on the other hand, since our main goal here is not to impose specific constraints on the ALP parameter space, we have assigned typical values to some of these parameters. As we use the same magnetic field model parameters for each EBL model, our main conclusions will not be affected.

IV. ANALYSIS AND RESULTS

In this section, we show our analysis and results under the ALP assumption with the different EBL spectral models. After considering the above photon-ALP conversion effect, we can derive the final photon survival probability $\mathcal{P}_{\gamma\gamma}$, then the chi-square value under the ALP assumption is given by

$$\chi_{\text{ALP}}^2 = \sum_{i=1}^N \left(\frac{\mathcal{P}_{\gamma\gamma} \Phi_{\text{int}}(E_i) - \psi(E_i)}{\delta(E_i)} \right)^2. \quad (18)$$

Notice that in the calculations the EBL absorption effect in the extragalactic space is also included in the final photon survival probability. For one ALP $\{m_a, g_{a\gamma}\}$ parameter set, we can derive one best-fit χ_{ALP}^2 under the ALP assumption, and also the best-fit χ_{ALP}^2 distribution in the whole ALP parameter plane. By utilizing this chi-square distribution, we can obtain the $\Delta\chi_{\text{ALP}}^2$ at the particular confidence level to establish the corresponding ALP bound. However, in this work, we do not intend to set any limits on ALP, but rather focus on the EBL absorption effect using different EBL spectral models.

We first show in figures 3 and 4 the best-fit chi-square χ_{ALP}^2 distributions of Markarian 501, 1ES 0229+200, PKS 0301-243, and PKS 0447-439 under the ALP assumption in the $\{m_a, g_{a\gamma}\}$ plane. The three EBL spectral models Finke-10, Franceschini-17, and Saldana-Lopez-21 are arranged from top to bottom. When comparing the panels

TABLE IV. The blazar jet magnetic field model parameters of Markarian 501, 1ES 0229+200, PKS 0301-243, and PKS 0447-439.

Source	B_0 (mG)	R_{VHE} (10^{17} cm)	θ_{jet} (deg)	r_{VHE} (10^{17} cm)	δ_{D}	ref.
Markarian 501	20	1.0	3.0	19.1	13	[54]
1ES 0229+200	~ 2	~ 0.2	2.5	4.6	~ 50	[79]
PKS 0301-243	20	1.3	~ 2	37.2	27	[56]
PKS 0447-439	20	0.65	~ 2	18.6	~ 51	[57]

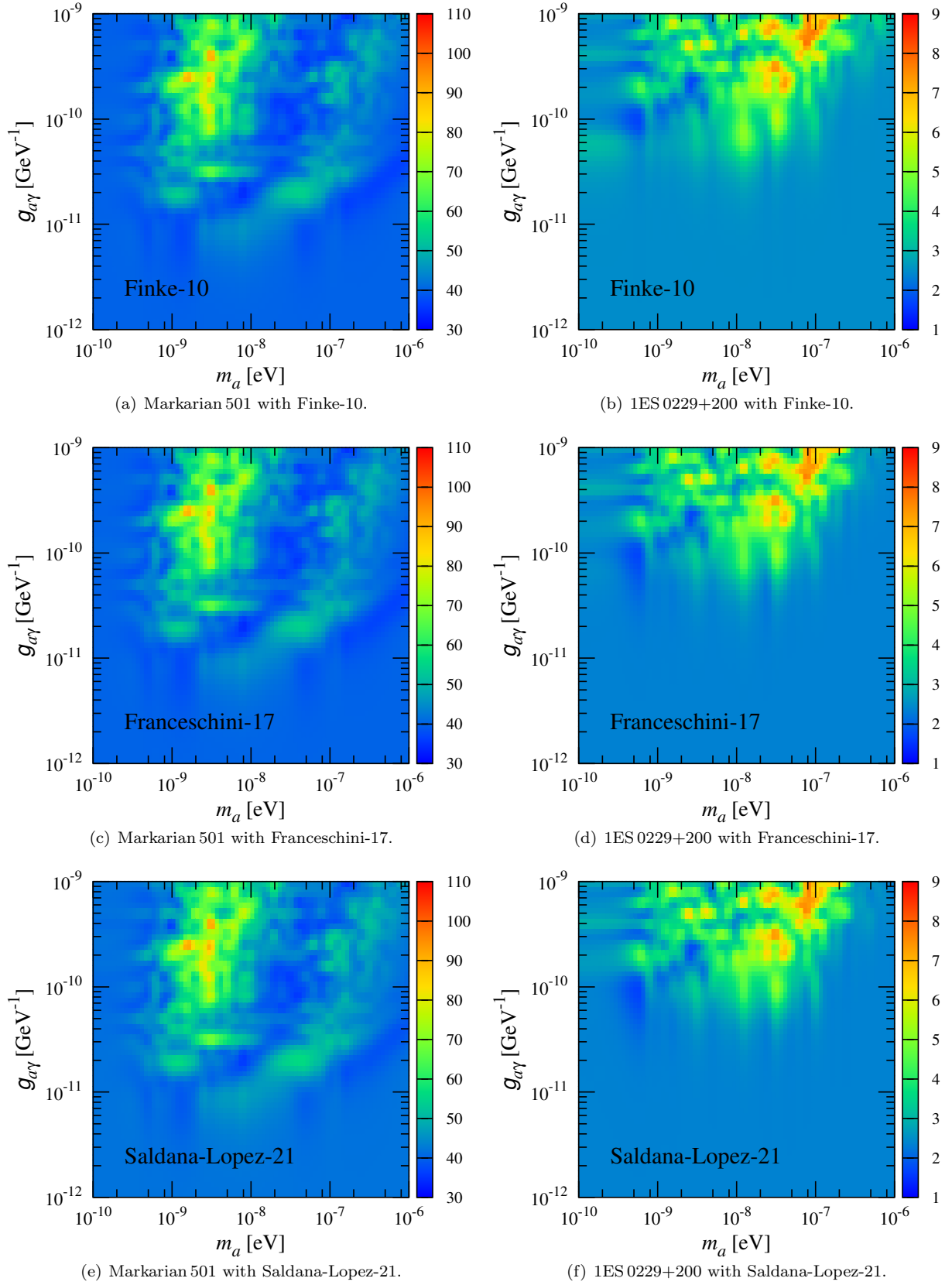
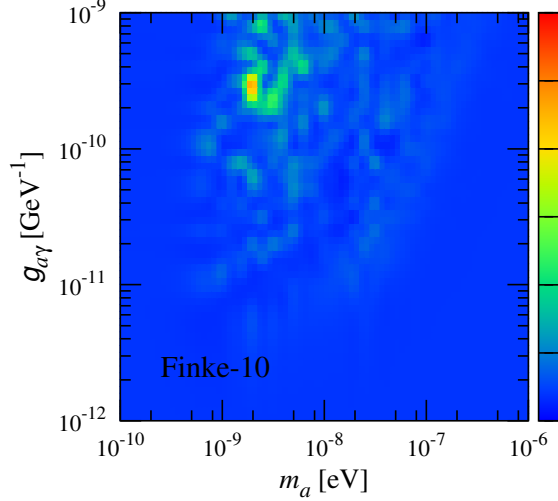
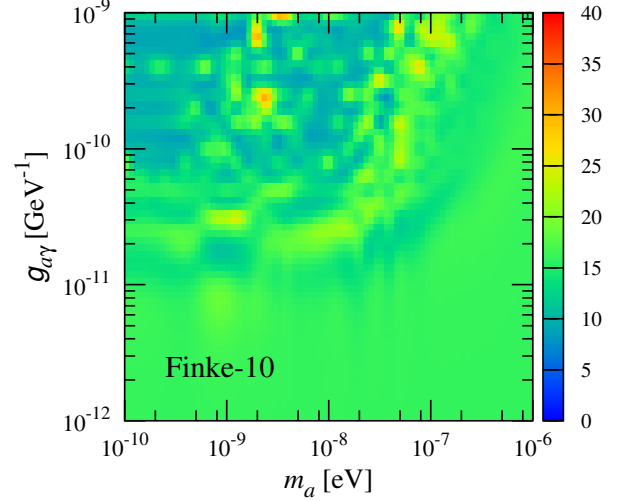


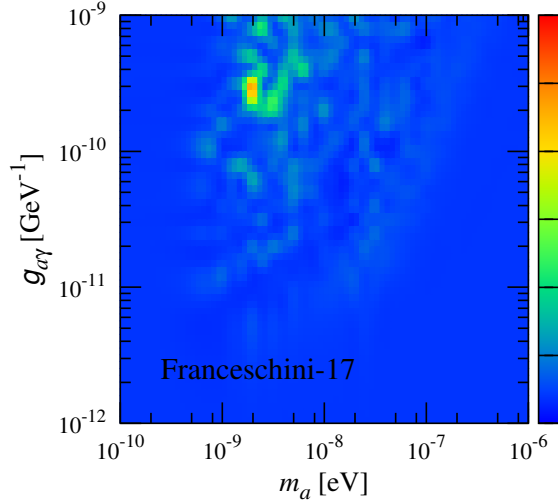
FIG. 3. The best-fit ALP assumption chi-square χ_{ALP}^2 distributions. The left and right panels correspond to Markarian 501 and 1ES 0229+200, respectively. The top, middle, and bottom panels correspond to the EBL models Finke-10, Franceschini-17, and Saldana-Lopez-21, respectively.



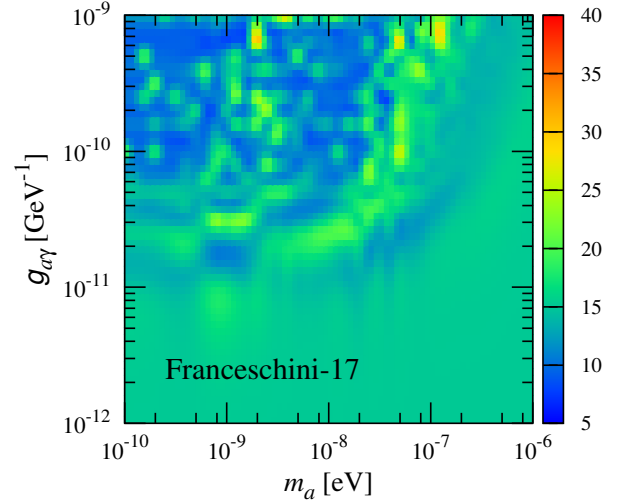
(a) PKS 0301-243 with Finke-10.



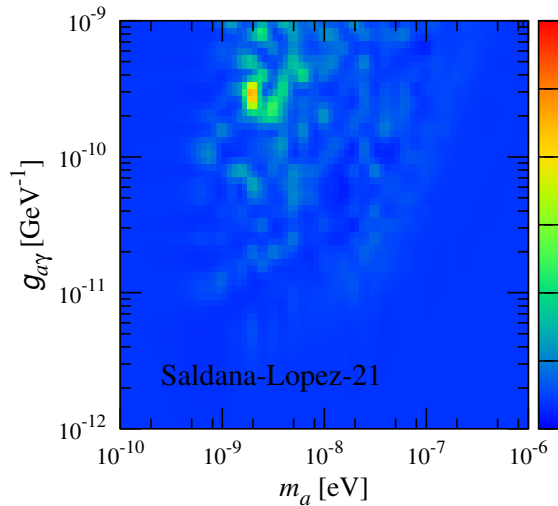
(b) PKS 0447-439 with Finke-10.



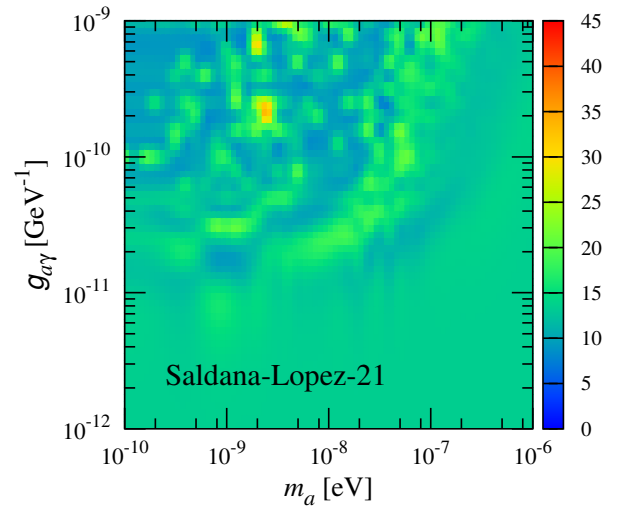
(c) PKS 0301-243 with Franceschini-17.



(d) PKS 0447-439 with Franceschini-17.



(e) PKS 0301-243 with Saldana-Lopez-21.



(f) PKS 0447-439 with Saldana-Lopez-21.

FIG. 4. The best-fit ALP assumption chi-square χ_{ALP}^2 distributions. The left and right panels correspond to PKS 0301-243 and PKS 0447-439, respectively. The top, middle, and bottom panels correspond to the EBL models Finke-10, Franceschini-17, and Saldana-Lopez-21, respectively.

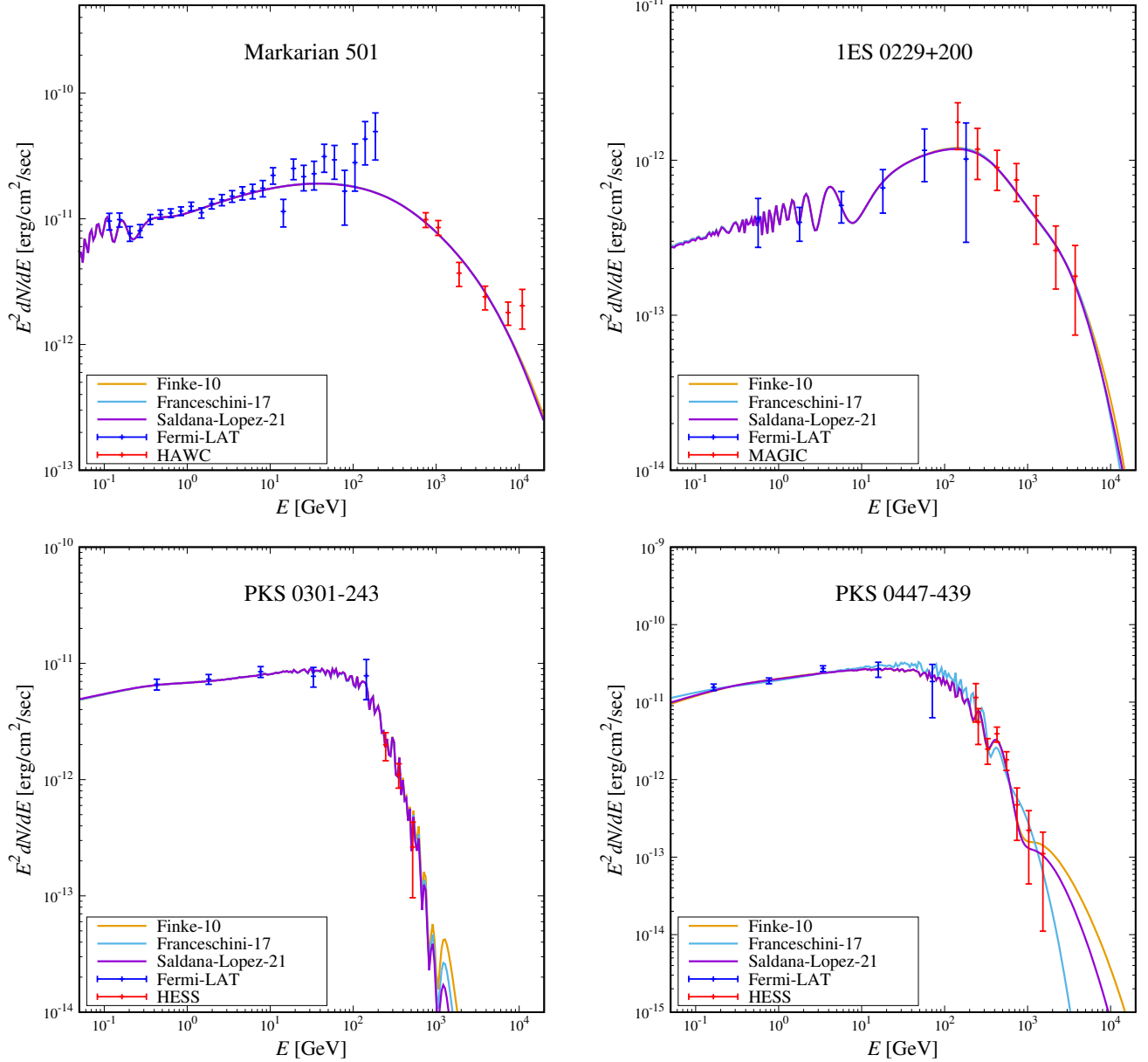


FIG. 5. The best-fit ALP assumption gamma-ray SEDs corresponding to χ_{\min}^2 of Markarian 501, 1ES 0229+200, PKS 0301-243, and PKS 0447-439. The yellow, blue, and purple lines correspond to the SEDs with the EBL spectral models Finke-10, Franceschini-17, and Saldana-Lopez-21, respectively. The blue and red points represent the experimental data.

for the same source, we find that there are no significant changes in the χ_{ALP}^2 values for the same parameter set across different EBL spectral models. Here the minimum best-fit chi-square in the $\{m_a, g_{a\gamma}\}$ plane can be defined as χ_{\min}^2 , which are listed in table V. For the sources Markarian 501, 1ES 0229+200, and PKS 0301-243, we find that the ALP parameter points corresponding to χ_{\min}^2 from the three different EBL models all coincide at the same point. However, for PKS 0447-439, only two of the EBL models have their minimum chi-square values corresponding to the same location. Next we show in figure 5 the gamma-ray SEDs corresponding to χ_{\min}^2 . We find that for the sources Markarian 501 and 1ES 0229+200, the SEDs corresponding to different EBL models are almost identical. However, for the sources PKS 0301-243 and PKS 0447-439, there are certain differences in their distributions at high-energy ranges, particularly for PKS 0447-439. The noticeable variations in the SEDs of PKS 0447-439 can be partly attributed to the different magnetic field configuration (resulting from different ALP parameter points) corresponding to the EBL model Franceschini-17 and, additionally, to the high redshift of PKS 0447-439.

Therefore, in order to characterize the difference in chi-square between the three different EBL spectral models in

this work, it is necessary to define a new delta chi-square for each $\{m_a, g_{a\gamma}\}$ set

$$\begin{aligned}\chi_d^2 &= \frac{1}{6} \sum_{i=1}^3 \sum_{j=1}^3 (1 - \delta_{ij}) \left| \chi_{\text{ALP},i}^2 - \chi_{\text{ALP},j}^2 \right| \\ &= \frac{1}{3} \left(\left| \chi_{\text{ALP},1}^2 - \chi_{\text{ALP},2}^2 \right| + \left| \chi_{\text{ALP},1}^2 - \chi_{\text{ALP},3}^2 \right| + \left| \chi_{\text{ALP},2}^2 - \chi_{\text{ALP},3}^2 \right| \right),\end{aligned}\quad (19)$$

where i and j represent the number of the three EBL models, and δ_{ij} is the Kronecker delta function

$$\delta_{ij} = \begin{cases} 1, & i = j \\ 0, & i \neq j \end{cases} \quad (20)$$

Notice that eq. (19) is only used to quantify the chi-square variation, and any subtle chi-square differences among the three EBL spectral models can be reflected by this value. Figure 6 shows the distributions of this delta chi-square in the $\{m_a, g_{a\gamma}\}$ plane of Markarian 501, 1ES 0229+200, PKS 0301-243, and PKS 0447-439, respectively. From this plot, we can clearly observe the chi-square differences and their corresponding ALP parameter points. The results indicate that across the entire parameter plane, the chi-square values of the sources Markarian 501, 1ES 0229+200, and PKS 0301-243 are consistently small and remain below 2. Conversely, within the same parameter plane, PKS 0447-439 demonstrates numerous chi-square values that are significantly larger. Here the maximum delta chi-square in the $\{m_a, g_{a\gamma}\}$ plane can be defined as $\chi_{d,\text{max}}^2$, which are listed in table VI. Then we show in figure 7 the gamma-ray SEDs corresponding to $\chi_{d,\text{max}}^2$. We observe that for the sources Markarian 501 and PKS 0301-243, there is little difference in their SEDs across different EBL models. However, for 1ES 0229+200 and PKS 0447-439, under different EBL models, there are significant differences in the high-energy range. Note that for PKS 0447-439, the spectra displayed here are all for the same ALP parameter point, which differs from the distributions shown in figure 5.

V. CONCLUSION

In summary, we have investigated the impact of the EBL absorption effect on photon-ALP conversions from the VHE gamma-ray spectral irregularities. For our purpose, we select four BL Lac blazars: Markarian 501 ($z_0 = 0.034$), 1ES 0229+200 ($z_0 = 0.1396$), PKS 0301-243 ($z_0 = 0.2657$), and PKS 0447-439 ($z_0 = 0.343$). These gamma-ray sources have a relatively certain redshift, ranging from low to high, making them a suitable choice for exploring the impact of the EBL absorption effect. On the other hand, we select three EBL spectral models: Finke-10, Franceschini-17, and Saldana-Lopez-21. These models are the latest ones available, and there are distinct differences among them. More importantly, the observations for Saldana-Lopez-21 originate from space, providing greater reliability than those conducted from the Earth.

We first discuss the EBL absorption effect on the gamma-ray SEDs with these three EBL spectral models. Then we consider the photon-ALP conversions in astrophysical magnetic fields. This includes a discussion on photon-ALP

TABLE V. The minimum best-fit ALP assumption chi-square χ_{min}^2 values of Markarian 501, 1ES 0229+200, PKS 0301-243, and PKS 0447-439 with the EBL spectral models Finke-10, Franceschini-17, and Saldana-Lopez-21.

Source	EBL model	χ_{min}^2	m_a (eV)	$g_{a\gamma}$ (GeV^{-1})
Markarian 501 (33 points)	Finke-10	30.52	1.0×10^{-9}	4.0×10^{-10}
	Franceschini-17	30.66	1.0×10^{-9}	4.0×10^{-10}
	Saldana-Lopez-21	30.90	1.0×10^{-9}	4.0×10^{-10}
1ES 0229+200 (13 points)	Finke-10	1.46	2.5×10^{-9}	2.0×10^{-10}
	Franceschini-17	1.46	2.5×10^{-9}	2.0×10^{-10}
	Saldana-Lopez-21	1.50	2.5×10^{-9}	2.0×10^{-10}
PKS 0301-243 (8 points)	Finke-10	0.48	1.0×10^{-7}	6.3×10^{-10}
	Franceschini-17	0.48	1.0×10^{-7}	6.3×10^{-10}
	Saldana-Lopez-21	0.52	1.0×10^{-7}	6.3×10^{-10}
PKS 0447-439 (13 points)	Finke-10	4.79	3.2×10^{-8}	1.6×10^{-10}
	Franceschini-17	5.92	4.0×10^{-8}	4.0×10^{-10}
	Saldana-Lopez-21	4.64	3.2×10^{-8}	1.6×10^{-10}

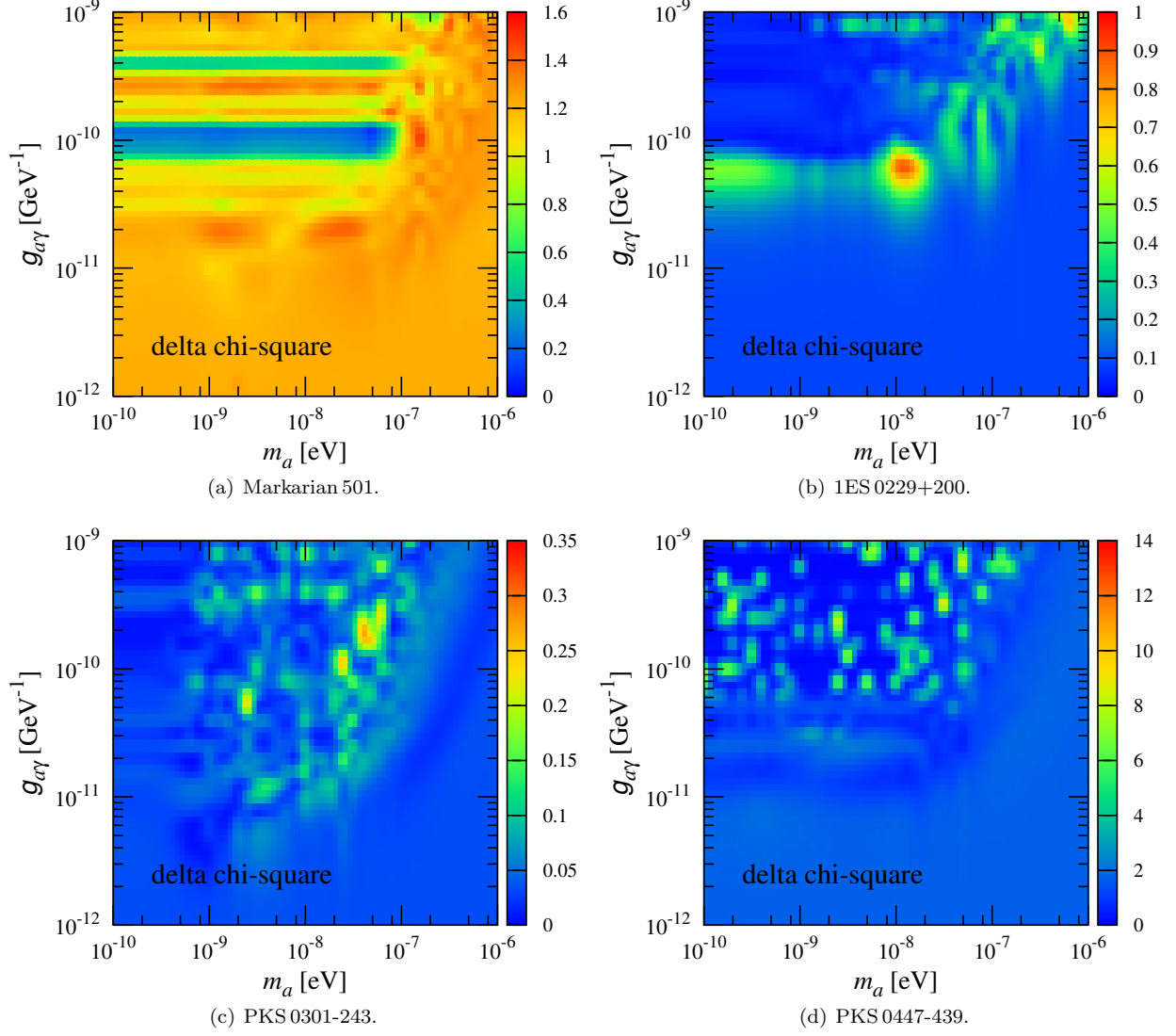


FIG. 6. The delta chi-square χ_d^2 distributions of Markarian 501, 1ES 0229+200, PKS 0301-243, and PKS 0447-439.

TABLE VI. The maximum delta chi-square $\chi_{d,\max}^2$ values of Markarian 501, 1ES 0229+200, PKS 0301-243, and PKS 0447-439.

Source	$\chi_{d,\max}^2$	m_a (eV)	$g_{a\gamma}$ (GeV^{-1})
Markarian 501	1.59	1.6×10^{-7}	1.0×10^{-10}
1ES 0229+200	0.95	1.3×10^{-8}	6.3×10^{-11}
PKS 0301-243	0.31	4.0×10^{-8}	2.0×10^{-10}
PKS 0447-439	13.00	3.2×10^{-8}	3.2×10^{-10}

conversions in both inhomogeneous magnetic fields and the astrophysical magnetic field configurations. The best-fit chi-square distributions of these EBL models under the ALP assumption in the ALP parameter $\{m_a, g_{a\gamma}\}$ plane are given (see figure 2), showing similar distributions. From the gamma-ray SEDs corresponding to χ_{\min}^2 , we find that for Markarian 501 and 1ES 0229+200, the SEDs corresponding to different EBL models are almost identical. However, for PKS 0301-243 and PKS 0447-439, there are certain differences in their distributions at high-energy ranges. For comparison, we define a new delta chi-square χ_d^2 to quantify the chi-square difference. The distributions of χ_d^2 and the gamma-ray SEDs corresponding to the maximum delta chi-square $\chi_{d,\max}^2$ in the $\{m_a, g_{a\gamma}\}$ plane are also shown (see figures 3, 4, and 6). Finally, we find that there is only a minor influence from the different EBL models at

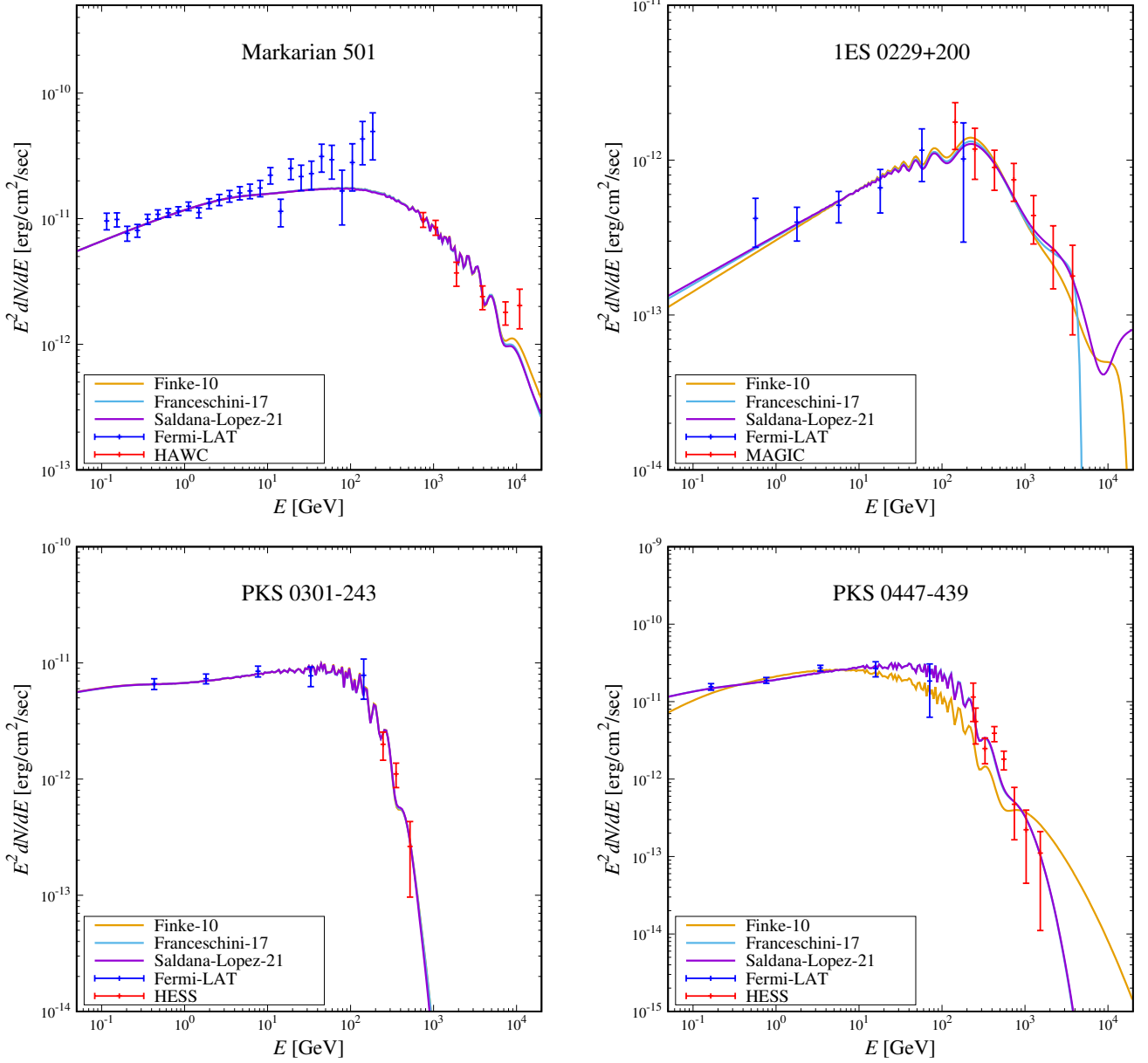


FIG. 7. The best-fit ALP assumption gamma-ray SEDs corresponding to $\chi^2_{d,\max}$ of Markarian 501, 1ES 0229+200, PKS 0301-243, and PKS 0447-439. The yellow, blue, and purple lines correspond to the SEDs with the EBL spectral models Finke-10, Franceschini-17, and Saldana-Lopez-21, respectively. The blue and red points represent the experimental data.

the low-redshift gamma-ray axionoscope. However, as the redshift of the sources increases, this impact becomes more pronounced, which can be observed from the gamma-ray SEDs (see figures 5 and 7). On the other hand, the uncertainty in the observed spectra can also directly affect the results. Overall, for the investigation of photon-ALP coupling from the low-redshift gamma-ray sources, the selection of the EBL spectral model Saldana-Lopez-21 is sufficient, as it provides a reliable absorption model for this scenario. Additionally, this absorption effect is expected to become more significant in the next generation of higher-energy gamma-ray observation experiments.

Acknowledgments.—W.C. is supported by the National Key R&D Program of China (Grant No. 2023YFA1607104), the National Natural Science Foundation of China (NSFC) (Grants No. 11775025 and No. 12175027), and the Fundamental Research Funds for the Central Universities (Grant No. 2017NT17). Y.F.Z. is supported by the National Key R&D Program of China (Grant No. 2017YFA0402204), the CAS Project for Young Scientists in Basic Research YSBR-006, and the NSFC (Grants No. 11821505, No. 11825506, and No. 12047503).

Appendix A: General photon-ALP conversions

Here we present the general photon-ALP conversions in the homogeneous magnetic field and the calculation of the photon-ALP conversion probability [38, 72, 80]. The photon-ALP system (A_1 , A_2 , and a) can be described by

$$\psi(x_3) = \begin{pmatrix} A_1(x_3) \\ A_2(x_3) \\ a(x_3) \end{pmatrix}, \quad (\text{A1})$$

where x_3 is the direction of propagation, A_1 and A_2 represent the linear polarization amplitudes of the photons in the perpendicular directions (x_1, x_2)

$$|A_1\rangle = \begin{pmatrix} 1 \\ 0 \\ 0 \end{pmatrix}, \quad |A_2\rangle = \begin{pmatrix} 0 \\ 1 \\ 0 \end{pmatrix}, \quad |a\rangle = \begin{pmatrix} 0 \\ 0 \\ 1 \end{pmatrix}. \quad (\text{A2})$$

Then the equation of motion for the photon-ALP system in the magnetic field can be described by

$$\left(i \frac{d}{dx_3} + E + \mathcal{M}(E, x_3) \right) \psi(x_3) = 0, \quad (\text{A3})$$

where E is the photon-ALP beam energy, and $\mathcal{M}(E, x_3)$ is the mixing matrix

$$\mathcal{M}(E, x_3) = \begin{pmatrix} \Delta_{11}(E, x_3) & \Delta_{12}(E, x_3) & \Delta_{a\gamma,1}(x_3) \\ \Delta_{21}(E, x_3) & \Delta_{22}(E, x_3) & \Delta_{a\gamma,2}(x_3) \\ \Delta_{a\gamma,1}(x_3) & \Delta_{a\gamma,2}(x_3) & \Delta_{aa}(E) \end{pmatrix}. \quad (\text{A4})$$

These terms are given by

$$\Delta_{11}(E, x_3) = \Delta_{\text{pl}}(E, x_3) + 2\Delta_{\text{QED}}(E, x_3) + \Delta_{\text{CMB}}(E), \quad (\text{A5})$$

$$\Delta_{22}(E, x_3) = \Delta_{\text{pl}}(E, x_3) + \frac{7}{2}\Delta_{\text{QED}}(E, x_3) + \Delta_{\text{CMB}}(E), \quad (\text{A6})$$

with

$$\Delta_{\text{pl}}(E, x_3) = -\frac{\omega_{\text{pl}}^2(x_3)}{2E} \simeq -1.08 \times 10^{-1} \left(\frac{n_e}{\text{cm}^{-3}} \right) \left(\frac{E}{1 \text{ GeV}} \right)^{-1} \text{ Mpc}^{-1}, \quad (\text{A7})$$

$$\Delta_{\text{QED}}(E, x_3) = \frac{\alpha E}{45\pi} \left(\frac{B_T(x_3)}{B_{\text{cr}}} \right)^2 \simeq 4.10 \times 10^{-12} \left(\frac{E}{1 \text{ GeV}} \right) \left(\frac{B_T(x_3)}{1 \text{ nG}} \right)^2 \text{ Mpc}^{-1}, \quad (\text{A8})$$

$$\Delta_{\text{CMB}}(E) = \rho_{\text{CMB}} E \simeq 0.80 \times 10^{-4} \left(\frac{E}{1 \text{ GeV}} \right) \text{ Mpc}^{-1}, \quad (\text{A9})$$

$$\Delta_{a\gamma}(x_3) = \frac{1}{2} g_{a\gamma} B_T(x_3) \simeq 1.52 \times 10^{-2} \left(\frac{g_{a\gamma}}{10^{-11} \text{ GeV}^{-1}} \right) \left(\frac{B_T(x_3)}{1 \text{ nG}} \right) \text{ Mpc}^{-1}, \quad (\text{A10})$$

$$\Delta_{aa}(E) = -\frac{m_a^2}{2E} \simeq -0.78 \times 10^2 \left(\frac{m_a}{10^{-9} \text{ GeV}} \right)^2 \left(\frac{E}{1 \text{ GeV}} \right)^{-1} \text{ Mpc}^{-1}. \quad (\text{A11})$$

Note that the Faraday rotation terms $\Delta_{12}(E, x_3)$ and $\Delta_{21}(E, x_3)$ can be neglected. Here the term $\Delta_{\text{pl}}(E, x_3)$ represents the plasma effect when the photon-ALP system propagates in the plasma environment with the plasma frequency

$$\omega_{\text{pl}} = \sqrt{\frac{4\pi\alpha n_e}{m_e}}, \quad (\text{A12})$$

where α is the fine-structure constant, n_e and m_e are the free electron number density and mass, respectively. The term $\Delta_{\text{QED}}(E, x_3)$ represents the QED vacuum polarization effect with the critical magnetic field [81]

$$B_{\text{cr}} = \frac{m_e^2}{|e|} \simeq 4.41 \times 10^{13} \text{ G}, \quad (\text{A13})$$

and the term $\Delta_{\text{CMB}}(E, x_3)$ represents the CMB photon dispersion effect with [82]

$$\rho_{\text{CMB}} \simeq 0.511 \times 10^{-42}. \quad (\text{A14})$$

If considering the transversal magnetic field B_T is aligned along the direction x_2 , the mixing matrix $\mathcal{M}(E, x_3)$ can be rewritten as

$$\mathcal{M}(E, x_3) = \begin{pmatrix} \Delta_{11}(E, x_3) & 0 & 0 \\ 0 & \Delta_{22}(E, x_3) & \Delta_{a\gamma}(x_3) \\ 0 & \Delta_{a\gamma}(x_3) & \Delta_{aa}(E) \end{pmatrix}. \quad (\text{A15})$$

Finally, the photon-ALP conversion probability in the homogeneous magnetic field can be described by

$$\mathcal{P}_{a\gamma}(E, x_3) = \left(\frac{g_{a\gamma} B_T L_{\text{osc}}(E)}{2\pi} \right)^2 \sin^2 \left(\frac{\pi x_3}{L_{\text{osc}}(E)} \right), \quad (\text{A16})$$

where $L_{\text{osc}}(E)$ is the oscillation length

$$\begin{aligned} L_{\text{osc}}(E) &= 2\pi \left[(\Delta_{22}(E) - \Delta_{aa}(E))^2 + 4\Delta_{a\gamma}^2 \right]^{-1/2} \\ &= 2\pi \left[\left[\frac{|m_a^2 - \omega_{\text{pl}}^2|}{2E} + E \left(\frac{7\alpha}{90\pi} \left(\frac{B_T}{B_{\text{cr}}} \right)^2 + \rho_{\text{CMB}} \right) \right]^2 + g_{a\gamma}^2 B_T^2 \right]^{-1/2}. \end{aligned} \quad (\text{A17})$$

-
- [1] R. Peccei and H. R. Quinn, CP Conservation in the Presence of Instantons, *Phys. Rev. Lett.* **38**, 1440 (1977).
 - [2] R. Peccei and H. R. Quinn, Constraints Imposed by CP Conservation in the Presence of Instantons, *Phys. Rev. D* **16**, 1791 (1977).
 - [3] S. Weinberg, A New Light Boson?, *Phys. Rev. Lett.* **40**, 223 (1978).
 - [4] F. Wilczek, Problem of Strong P and T Invariance in the Presence of Instantons, *Phys. Rev. Lett.* **40**, 279 (1978).
 - [5] J. Preskill, M. B. Wise, and F. Wilczek, Cosmology of the Invisible Axion, *Phys. Lett. B* **120**, 127 (1983).
 - [6] L. Abbott and P. Sikivie, A Cosmological Bound on the Invisible Axion, *Phys. Lett. B* **120**, 133 (1983).
 - [7] M. Dine and W. Fischler, The Not So Harmless Axion, *Phys. Lett. B* **120**, 137 (1983).
 - [8] A. Arvanitaki, S. Dimopoulos, S. Dubovsky, N. Kaloper, and J. March-Russell, String Axiverse, *Phys. Rev. D* **81**, 123530 (2010), [arXiv:0905.4720 \[hep-th\]](#).
 - [9] P. Svrcek and E. Witten, Axions In String Theory, *JHEP* **06**, 051, [arXiv:hep-th/0605206](#).
 - [10] D. Cadamuro and J. Redondo, Cosmological bounds on pseudo Nambu-Goldstone bosons, *JCAP* **02**, 032, [arXiv:1110.2895 \[hep-ph\]](#).
 - [11] P. Arias, D. Cadamuro, M. Goodsell, J. Jaeckel, J. Redondo, and A. Ringwald, WISPy Cold Dark Matter, *JCAP* **06**, 013, [arXiv:1201.5902 \[hep-ph\]](#).
 - [12] W. Chao, M. Jin, H.-J. Li, Y.-Q. Peng, and Y. Wang, Axionlike dark matter from the type-II seesaw mechanism, *Phys. Rev. D* **109**, 115027 (2024), [arXiv:2210.13233 \[hep-ph\]](#).
 - [13] C. O'HARE, [cajohare/axionlimits: Axionlimits](#) (2020).
 - [14] A. De Angelis, M. Roncadelli, and O. Mansutti, Evidence for a new light spin-zero boson from cosmological gamma-ray propagation?, *Phys. Rev. D* **76**, 121301 (2007), [arXiv:0707.4312 \[astro-ph\]](#).
 - [15] A. Mirizzi, G. G. Raffelt, and P. D. Serpico, Signatures of Axion-Like Particles in the Spectra of TeV Gamma-Ray Sources, *Phys. Rev. D* **76**, 023001 (2007), [arXiv:0704.3044 \[astro-ph\]](#).
 - [16] M. Simet, D. Hooper, and P. D. Serpico, The Milky Way as a Kiloparsec-Scale Axionscope, *Phys. Rev. D* **77**, 063001 (2008), [arXiv:0712.2825 \[astro-ph\]](#).
 - [17] D. Hooper and P. D. Serpico, Detecting Axion-Like Particles With Gamma Ray Telescopes, *Phys. Rev. Lett.* **99**, 231102 (2007), [arXiv:0706.3203 \[hep-ph\]](#).
 - [18] F. Aharonian et al. (H.E.S.S.), New constraints on the Mid-IR EBL from the HESS discovery of VHE gamma rays from 1ES 0229+200, *Astron. Astrophys.* **475**, L9 (2007), [arXiv:0709.4584 \[astro-ph\]](#).
 - [19] E. Aliu et al. (MAGIC), Very-High-Energy Gamma Rays from a Distant Quasar: How Transparent Is the Universe?, *Science* **320**, 1752 (2008), [arXiv:0807.2822 \[astro-ph\]](#).
 - [20] A. Abramowski et al. (H.E.S.S.), Constraints on axionlike particles with H.E.S.S. from the irregularity of the PKS 2155-304 energy spectrum, *Phys. Rev. D* **88**, 102003 (2013), [arXiv:1311.3148 \[astro-ph.HE\]](#).
 - [21] M. Ajello et al. (Fermi-LAT), Search for Spectral Irregularities due to Photon-Axionlike-Particle Oscillations with the Fermi Large Area Telescope, *Phys. Rev. Lett.* **116**, 161101 (2016), [arXiv:1603.06978 \[astro-ph.HE\]](#).
 - [22] K. Kohri and H. Kodama, Axion-Like Particles and Recent Observations of the Cosmic Infrared Background Radiation, *Phys. Rev. D* **96**, 051701 (2017), [arXiv:1704.05189 \[hep-ph\]](#).

- [23] C. Zhang, Y.-F. Liang, S. Li, N.-H. Liao, L. Feng, Q. Yuan, Y.-Z. Fan, and Z.-Z. Ren, New bounds on axionlike particles from the Fermi Large Area Telescope observation of PKS 2155-304, *Phys. Rev. D* **97**, 063009 (2018), [arXiv:1802.08420 \[hep-ph\]](#).
- [24] M. M. Ivanov, Y. Y. Kovalev, M. L. Lister, A. G. Panin, A. B. Pushkarev, T. Savolainen, and S. V. Troitsky, Constraining the photon coupling of ultra-light dark-matter axion-like particles by polarization variations of parsec-scale jets in active galaxies, *JCAP* **02**, 059, [arXiv:1811.10997 \[astro-ph.CO\]](#).
- [25] Y.-F. Liang, C. Zhang, Z.-Q. Xia, L. Feng, Q. Yuan, and Y.-Z. Fan, Constraints on axion-like particle properties with TeV gamma-ray observations of Galactic sources, *JCAP* **06**, 042, [arXiv:1804.07186 \[hep-ph\]](#).
- [26] M. Libanov and S. Troitsky, On the impact of magnetic-field models in galaxy clusters on constraints on axion-like particles from the lack of irregularities in high-energy spectra of astrophysical sources, *Phys. Lett. B* **802**, 135252 (2020), [arXiv:1908.03084 \[astro-ph.HE\]](#).
- [27] G. Long, W. Lin, P. Tam, and W. Zhu, Testing the CIBER cosmic infrared background measurements and axionlike particles with observations of TeV blazars, *Phys. Rev. D* **101**, 063004 (2020), [arXiv:1912.05309 \[astro-ph.HE\]](#).
- [28] J. Guo, H.-J. Li, X.-J. Bi, S.-J. Lin, and P.-F. Yin, The implications of the axion like particle from the Fermi-LAT and H.E.S.S. observations of PG 1553+113 and PKS 2155-304, *Chin. Phys. C* **45**, 025105 (2021), [arXiv:2002.07571 \[astro-ph.HE\]](#).
- [29] X.-J. Bi, Y. Gao, J. Guo, N. Houston, T. Li, F. Xu, and X. Zhang, Axion and dark photon limits from Crab Nebula high energy gamma-rays, *Phys. Rev. D* **103**, 043018 (2021), [arXiv:2002.01796 \[astro-ph.HE\]](#).
- [30] H.-J. Li, J.-G. Guo, X.-J. Bi, S.-J. Lin, and P.-F. Yin, Limits on axion-like particles from Mrk 421 with 4.5-year period observations by ARGO-YBJ and Fermi-LAT, *Phys. Rev. D* **103**, 083003 (2021), [arXiv:2008.09464 \[astro-ph.HE\]](#).
- [31] J.-G. Cheng, Y.-J. He, Y.-F. Liang, R.-J. Lu, and E.-W. Liang, Revisiting the analysis of axion-like particles with the Fermi-LAT gamma-ray observation of NGC1275, *Phys. Lett. B* **821**, 136611 (2021), [arXiv:2010.12396 \[astro-ph.HE\]](#).
- [32] H.-J. Li, X.-J. Bi, and P.-F. Yin, Searching for axion-like particles with the blazar observations of MAGIC and Fermi-LAT *, *Chin. Phys. C* **46**, 085105 (2022), [arXiv:2110.13636 \[astro-ph.HE\]](#).
- [33] H.-J. Li, Relevance of VHE blazar spectra models with axion-like particles, *JCAP* **02** (02), 025, [arXiv:2112.14145 \[astro-ph.HE\]](#).
- [34] C. Dessert, D. Dunskey, and B. R. Safdi, Upper limit on the axion-photon coupling from magnetic white dwarf polarization, *Phys. Rev. D* **105**, 103034 (2022), [arXiv:2203.04319 \[hep-ph\]](#).
- [35] H.-J. Li, Probing photon-ALP oscillations from the flat spectrum radio quasar 4C+21.35, *Phys. Lett. B* **829**, 137047 (2022), [arXiv:2203.08573 \[astro-ph.HE\]](#).
- [36] S. Jacobsen, T. Linden, and K. Freese, Constraining axion-like particles with HAWC observations of TeV blazars, *JCAP* **10**, 009, [arXiv:2203.04332 \[hep-ph\]](#).
- [37] L. Mastrototaro, P. Carenza, M. Chianese, D. F. G. Fiorillo, G. Miele, A. Mirizzi, and D. Montanino, Constraining axion-like particles with the diffuse gamma-ray flux measured by the Large High Altitude Air Shower Observatory, *Eur. Phys. J. C* **82**, 1012 (2022), [arXiv:2206.08945 \[hep-ph\]](#).
- [38] H.-J. Li, Primordial black holes induced stochastic axion-photon oscillations in primordial magnetic field, *JCAP* **11**, 045, [arXiv:2208.04605 \[astro-ph.CO\]](#).
- [39] D. Noordhuis, A. Prabhu, S. J. Witte, A. Y. Chen, F. Cruz, and C. Weniger, Novel Constraints on Axions Produced in Pulsar Polar-Cap Cascades, *Phys. Rev. Lett.* **131**, 111004 (2023), [arXiv:2209.09917 \[hep-ph\]](#).
- [40] B. P. Pant, Sunanda, R. Moharana, and S. S., Implications of photon-ALP oscillations in the extragalactic neutrino source TXS 0506+056 at sub-PeV energies, *Phys. Rev. D* **108**, 023016 (2023), [arXiv:2210.12652 \[astro-ph.HE\]](#).
- [41] L.-Q. Gao, X.-J. Bi, J.-G. Guo, W. Lin, and P.-F. Yin, Constraints on axionlike particles from observations of Mrk 421 using the CLs method, *Phys. Rev. D* **109**, 063003 (2024), [arXiv:2309.02166 \[astro-ph.HE\]](#).
- [42] B. P. Pant, Probing photon-ALP oscillations from the MAGIC observations of FSRQ QSO B1420+326, *Phys. Rev. D* **109**, 023011 (2024), [arXiv:2310.16634 \[astro-ph.HE\]](#).
- [43] B. P. Pant, Constraining axionlike particles with invisible neutrino decay using the IceCube observations of NGC 1068, *Phys. Rev. D* **109**, 063002 (2024), [arXiv:2311.14597 \[astro-ph.HE\]](#).
- [44] H.-J. Li, W. Chao, and Y.-F. Zhou, Axion limits from the 10-year gamma-ray emission 1ES 1215+303, *Phys. Lett. B* **850**, 138531 (2024), [arXiv:2312.05555 \[astro-ph.HE\]](#).
- [45] J. Li, X.-J. Bi, L.-Q. Gao, X. Huang, R.-M. Yao, and P.-F. Yin, Constraints on axion-like particles from the observation of Galactic sources by the LHAASO*, *Chin. Phys. C* **48**, 065107 (2024), [arXiv:2401.01829 \[astro-ph.HE\]](#).
- [46] W.-Q. Guo, Z.-Q. Xia, and X. Huang, Constraining axion-like particles dark matter in Coma Berenices with FAST, *Phys. Lett. B* **852**, 138631 (2024), [arXiv:2404.04881 \[astro-ph.HE\]](#).
- [47] H.-J. Li, W. Chao, and Y.-F. Zhou, Upper limit on the axion-photon coupling from Markarian 421, *Phys. Lett. B* **858**, 139075 (2024), [arXiv:2406.00387 \[hep-ph\]](#).
- [48] J. Ruz et al., NuSTAR as an Axion Helioscope, (2024), [arXiv:2407.03828 \[astro-ph.CO\]](#).
- [49] S. Porras-Bedmar, M. Meyer, and D. Horns, Novel bounds on decaying axion-like-particle dark matter from the cosmic background, (2024), [arXiv:2407.10618 \[astro-ph.CO\]](#).
- [50] L.-Q. Gao, X.-J. Bi, J. Li, and P.-F. Yin, Impact of Parameters in the Blazar Jet Magnetic Field Model on Axion-Like Particle Constraints, (2024), [arXiv:2407.20118 \[astro-ph.HE\]](#).
- [51] B. Betancourt Kamenetskaia, N. Fraija, and G. Herrera, Polarization Measurements as a Probe of Axion-Photon Coupling: a Study of GRB 221009A, (2024), [arXiv:2408.07352 \[hep-ph\]](#).
- [52] B.-Y. Zhu, X. Huang, and P.-F. Yin, Constraints on Axion-like Particles from the gamma-ray observation of the Galactic Center, (2024), [arXiv:2408.12234 \[astro-ph.HE\]](#).

- [53] H.-J. Li and W. Chao, Axion effects on gamma-ray spectral irregularities with AGN redshift uncertainty, *Phys. Rev. D* **107**, 063031 (2023), [arXiv:2211.00524 \[hep-ph\]](#).
- [54] A. Albert et al. (HAWC), Long-term Spectra of the Blazars Mrk 421 and Mrk 501 at TeV Energies Seen by HAWC, *Astrophys. J.* **929**, 125 (2022), [arXiv:2106.03946 \[astro-ph.HE\]](#).
- [55] V. A. Acciari et al. (MAGIC), A lower bound on intergalactic magnetic fields from time variability of 1ES 0229+200 from MAGIC and Fermi/LAT observations, *Astron. Astrophys.* **670**, A145 (2023), [arXiv:2210.03321 \[astro-ph.HE\]](#).
- [56] A. Abramowski et al. (H.E.S.S.), Discovery of very high energy gamma-ray emission from the BL Lac object PKS 0301-243 with H.E.S.S., *Astron. Astrophys.* **559**, A136 (2013), [arXiv:1309.6174 \[astro-ph.HE\]](#).
- [57] A. Abramowski et al. (HESS), Discovery of TeV γ -ray emission from PKS 0447-439 and derivation of an upper limit on its redshift, *Astron. Astrophys.* **552**, A118 (2013), [arXiv:1303.1628 \[astro-ph.HE\]](#).
- [58] J. D. Finke, S. Razzaque, and C. D. Dermer, Modeling the Extragalactic Background Light from Stars and Dust, *Astrophys. J.* **712**, 238 (2010), [arXiv:0905.1115 \[astro-ph.HE\]](#).
- [59] A. Franceschini and G. Rodighiero, The extragalactic background light revisited and the cosmic photon-photon opacity, *Astron. Astrophys.* **603**, A34 (2017), [arXiv:1705.10256 \[astro-ph.HE\]](#).
- [60] A. Saldana-Lopez, A. Domínguez, P. G. Pérez-González, J. Finke, M. Ajello, J. R. Primack, V. S. Paliya, and A. Desai, An observational determination of the evolving extragalactic background light from the multiwavelength HST/CANDELS survey in the Fermi and CTA era, *Mon. Not. Roy. Astron. Soc.* **507**, 5144 (2021), [arXiv:2012.03035 \[astro-ph.CO\]](#).
- [61] A. Franceschini, G. Rodighiero, and M. Vaccari, The extragalactic optical-infrared background radiations, their time evolution and the cosmic photon-photon opacity, *Astron. Astrophys.* **487**, 837 (2008), [arXiv:0805.1841 \[astro-ph\]](#).
- [62] S. Navas et al. (Particle Data Group), Review of particle physics, *Phys. Rev. D* **110**, 030001 (2024).
- [63] R. C. Gilmore, R. S. Somerville, J. R. Primack, and A. Dominguez, Semi-analytic modeling of the EBL and consequences for extragalactic gamma-ray spectra, *Mon. Not. Roy. Astron. Soc.* **422**, 3189 (2012), [arXiv:1104.0671 \[astro-ph.CO\]](#).
- [64] S. Matsuura et al., New Spectral Evidence of an Unaccounted Component of the Near-infrared Extragalactic Background Light from the CIBER, *Astrophys. J.* **839**, 7 (2017), [arXiv:1704.07166 \[astro-ph.GA\]](#).
- [65] J. Quinn et al., Detection of gamma-rays with $E > 300$ -GeV from Markarian 501, *Astrophys. J. Lett.* **456**, L83 (1996).
- [66] M. Elvis, D. Plummer, J. Schachter, and G. Fabbiano, The Einstein Slew Survey, *Astrophys. J. Suppl.* **80**, 257 (1992).
- [67] J. F. Schachter, J. T. Stocke, E. Perlman, M. Elvis, R. Remillard, A. Granados, J. Luu, J. P. Huchra, R. Humphreys, C. M. Urry, and J. Wallin, Ten New BL Lacertae Objects Discovered by an Efficient X-Ray/Radio/Optical Technique, *Astrophys. J.* **412**, 541 (1993).
- [68] C. D. Impey and S. Tapia, New Blazars Discovered by Polarimetry, *Astrophys. J.* **333**, 666 (1988).
- [69] G. Lamer, H. Brunner, and R. Staubert, ROSAT observations of BL Lacertae objects., *Astron. Astrophys.* **311**, 384 (1996), [arXiv:astro-ph/9603030 \[astro-ph\]](#).
- [70] M. I. Large, B. Y. Mills, A. G. Little, D. F. Crawford, and J. M. Sutton, The Molonglo Reference Catalogue of radio sources., *Mon. Not. Roy. Astron. Soc.* **194**, 693 (1981).
- [71] E. Perlman, P. Padovani, P. Giommi, R. Sambruna, L. R. Jones, A. Tzioumis, and J. Reynolds, The deep x-ray radio blazar survey (dxrbs). I. methods and first results, *Astron. J.* **115**, 1253 (1998), [arXiv:astro-ph/9801024](#).
- [72] A. De Angelis, G. Galanti, and M. Roncadelli, Relevance of axion-like particles for very-high-energy astrophysics, *Phys. Rev. D* **84**, 105030 (2011), [Erratum: *Phys.Rev.D* 87, 109903 (2013)], [arXiv:1106.1132 \[astro-ph.HE\]](#).
- [73] P. Ade et al. (Planck), Planck 2015 results. XIX. Constraints on primordial magnetic fields, *Astron. Astrophys.* **594**, A19 (2016), [arXiv:1502.01594 \[astro-ph.CO\]](#).
- [74] M. Pshirkov, P. Tinyakov, and F. Urban, New limits on extragalactic magnetic fields from rotation measures, *Phys. Rev. Lett.* **116**, 191302 (2016), [arXiv:1504.06546 \[astro-ph.CO\]](#).
- [75] R. Jansson and G. R. Farrar, A New Model of the Galactic Magnetic Field, *Astrophys. J.* **757**, 14 (2012), [arXiv:1204.3662 \[astro-ph.GA\]](#).
- [76] R. Jansson and G. R. Farrar, The Galactic Magnetic Field, *Astrophys. J. Lett.* **761**, L11 (2012), [arXiv:1210.7820 \[astro-ph.GA\]](#).
- [77] R. Adam et al. (Planck), Planck intermediate results.: XLII. Large-scale Galactic magnetic fields, *Astron. Astrophys.* **596**, A103 (2016), [arXiv:1601.00546 \[astro-ph.GA\]](#).
- [78] M. Unger and G. R. Farrar, The Coherent Magnetic Field of the Milky Way, *Astrophys. J.* **970**, 95 (2024), [arXiv:2311.12120 \[astro-ph.GA\]](#).
- [79] E. Aliu et al., A three-year multi-wavelength study of the very-high-energy γ -ray blazar 1ES 0229+200, *Astrophys. J.* **782**, 13 (2014), [arXiv:1312.6592 \[astro-ph.HE\]](#).
- [80] G. Raffelt and L. Stodolsky, Mixing of the Photon with Low Mass Particles, *Phys. Rev. D* **37**, 1237 (1988).
- [81] J. S. Schwinger, On gauge invariance and vacuum polarization, *Phys. Rev.* **82**, 664 (1951).
- [82] A. Dobrynina, A. Kartavtsev, and G. Raffelt, Photon-photon dispersion of TeV gamma rays and its role for photon-ALP conversion, *Phys. Rev. D* **91**, 083003 (2015), [Erratum: *Phys.Rev.D* 95, 109905 (2017)], [arXiv:1412.4777 \[astro-ph.HE\]](#).